Supporting Information for "Sensitivity-Enhanced Solid-state NMR Detection of Structural Differences and Unique Polymorphs in Pico- to Nanomolar Amounts of Brain-derived and Synthetic 42-residue Amyloid-β Fibrils"

Ayesha Wickramasinghe,[1, 2] Yiling Xiao,[4] Naohiro Kobayashi,[2, 3] Songlin Wang,[4] Kathryn P. Scherpelz,[5] Toshio Yamazaki,[2,3] Stephen C. Meredith,[5, 6] Yoshitaka Ishii[1, 2, 3, 4*]

[1] School of Life Science and Technology, Tokyo Institute of Technology, 4259 Nagatsuta-cho, Midori-ku, Yokohama, Kanagawa 226-8503, Japan

[2] NMR Division, RIKEN SPring-8 Center, RIKEN, 1-7-22 Suehiro-cho, Tsurumi-ku, Yokohama, Kanagawa 230-0045, Japan

[3] RIKEN Center for Biosystems Dynamics Research, RIKEN, 1-7-22 Suehiro-cho, Tsurumi-ku, Yokohama, Kanagawa 230-0045, Japan

[4]Department of Chemistry, University of Illinois at Chicago, Chicago, Illinois 60607, USA

[5]Department of Biochemistry and Molecular Biology, The University of Chicago, Chicago, Illinois 60637, USA

[6]Department of Pathology, The University of Chicago, Chicago, Illinois 60637, USA

Supplementary Figures

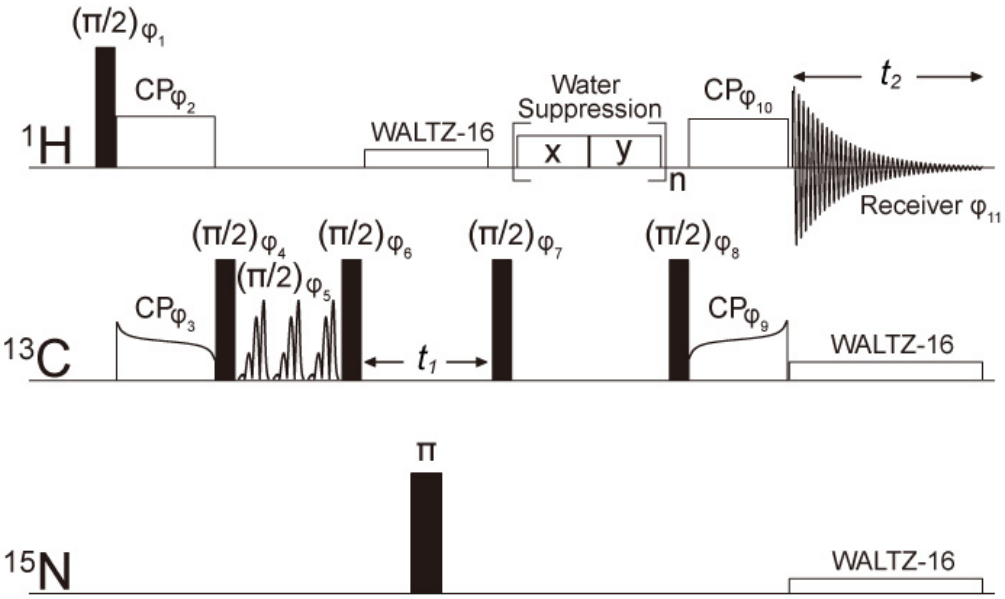

Figure S1. A pulse sequence used to record the ^{1}H-detected ^{13}C/^{1}H correlation 2D spectra in Figure 1a and b. In this sequence, ^{13}C spin polarization was prepared with adiabatic double-quantum cross polarization (DQ-CP). After applying a π/2-pulse to store the ^{13}C spin polarization along the static magnetic field, three E-Burp π/2-pulses were applied on the ^{13}C channel to selectively dephase ^{13}CO

and aromatic ^{13}C polarization before the t_1 evolution. For each E-burp pulse, the maximum field strength was 3.97 kHz and the pulse width was 0.42 ms. After the t_1 evolution, background or solvent ^{1}H signals from water were suppressed by MISSISSIPPI scheme.[1] The irradiation power and the pulse width were 20 kHz and 2 ms, respectively, and n was set to 4. Then, ^{13}C spin polarization was transferred back to ^{1}H spins with a second adiabatic DQ-CP. During the t_2 acquisition, ^{1}H signals were recorded with a dwell time of 5 μs under ^{13}C and ^{15}N decoupling. The phase cycle of the pulse sequence was as follows: φ_1 = y, y, -y, -y; φ_2 = x; φ_3 = x; φ_4 = y; φ_5 = y; φ_6 = y; φ_7 = y, -y; φ_8 = -y; φ_9 = x; φ_{10} = x; φ_{11} = -x, x, x, -x. φ_6 and φ_{11} were incremented during the t_1 evolution using the States-TPPI acquisition mode. Rest of the acquisition parameters can be found in the Materials and Methods section and Table S7.

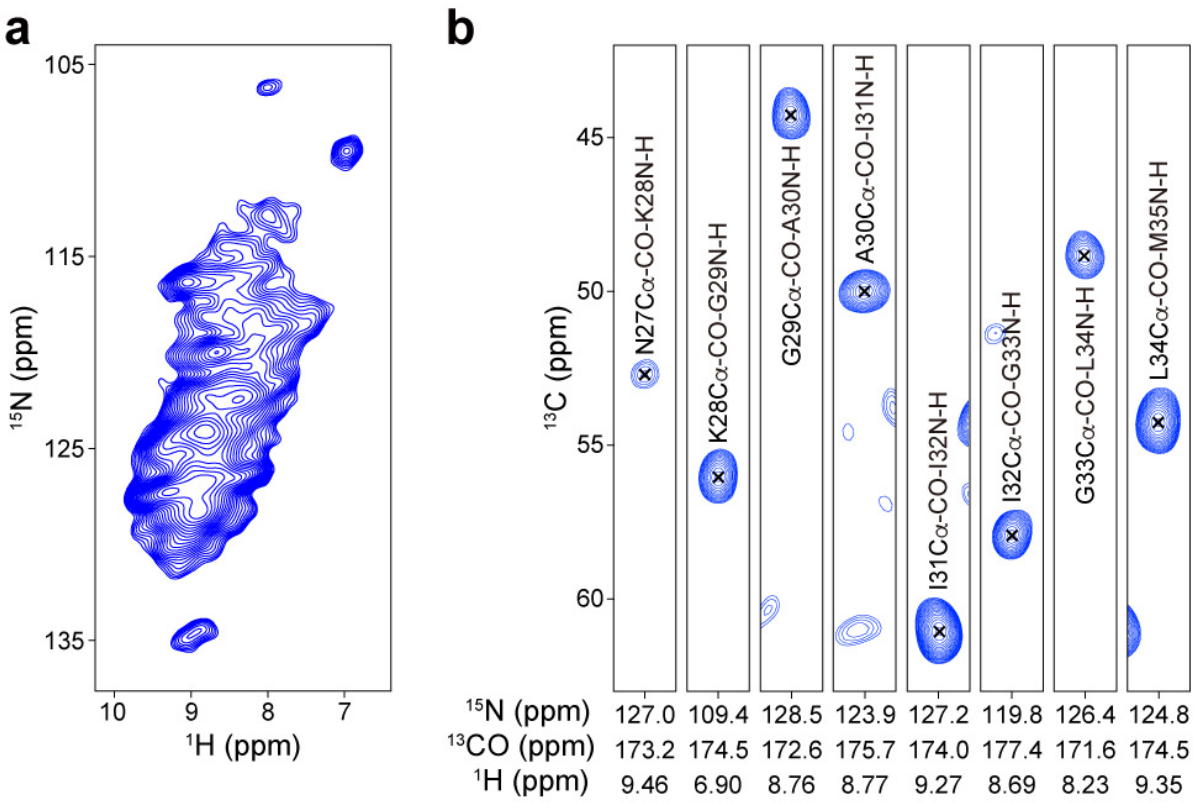

Figure S2. (a) ^{1}H-detected $^{15}N/^{1}H$ correlation 2D spectrum of uniformly ^{13}C- and ^{15}N-labeled Aβ42 fibril. As mentioned in the main text, the resolution is greatly limited with considerable signal overlapping. (b) Representative strip plots of (H)CACONH 4D spectrum for Lys-28 to Met-35 of uniformly ^{13}C- and ^{15}N-labeled Aβ42 fibril.

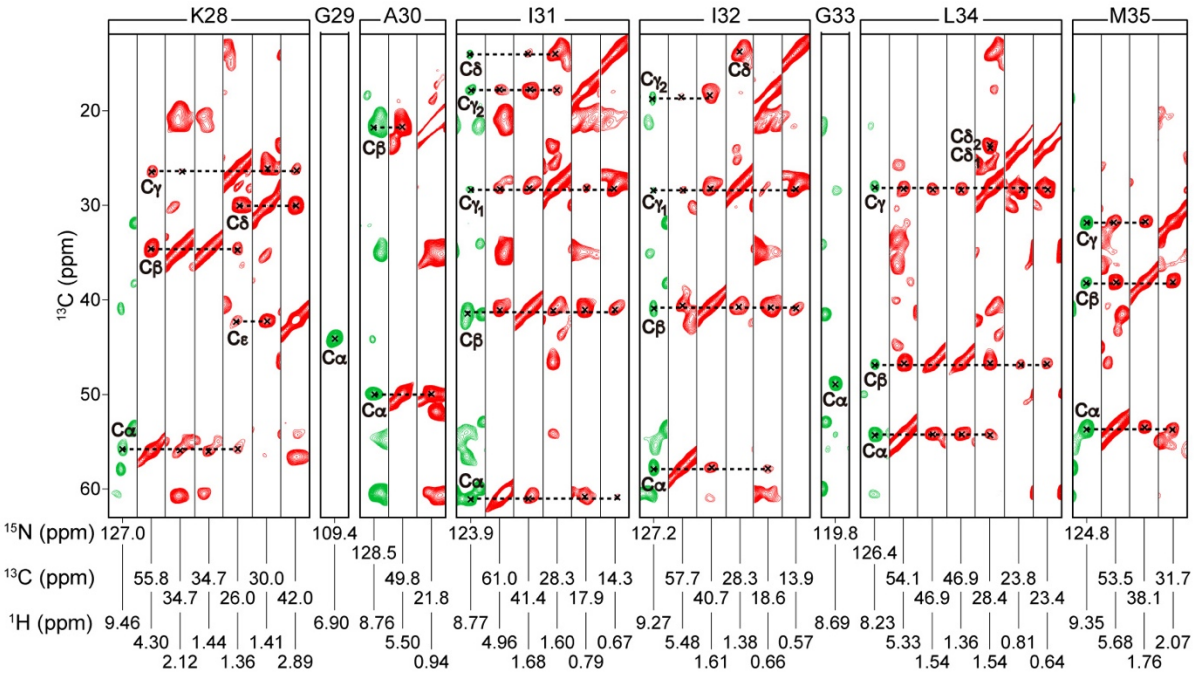

Figure S3. Representative strip plots of (H)CX(CA)NH (green) and (H)CCH (red) 3D spectra demonstrating the signal assignment of the aliphatic side-chain ^{13}C and ^{1}H for Lys-28 to Met-35 of uniformly ^{13}C- and ^{15}N-labeled Aβ42 fibril. We determined 88% of the resonances from the aliphatic side-chain ^{13}C by analyzing (H)CX(CA)NH and (H)CCH 3D spectra. Since we selectively quenched out the aromatic and carbonyl ^{13}C regions from the ^{13}C dimensions to maintain a reasonable experimental time by reducing the spectral width of the indirect dimensions, we did not observe any signals from aromatic or carbonyl side-chain ^{13}C in these spectra. However, we could assign some of the resonances corresponding to aromatic and carbonyl side-chain ^{13}C and the ^{13}CO resonance of Ala-42 in the ^{13}C/^{13}C correlation 2D spectrum acquired with RFDR mixing (data are not shown). Hence, all the assigned side-chain ^{13}C is 69% by taking aromatic and carbonyl side-chains into account, in addition to aliphatic side-chains. Furthermore, we assigned 62% of the ^{1}H resonances from the aliphatic side-chains of Aβ42 fibril, which do not include the side-chain ^{1}H chemical shifts of six Val residues and a few other residues. Since the signals corresponding to the correlations among side-chain ^{13}C and ^{1}H for Val residues are extensively overlapping with each other, it was difficult to decide the exact ^{1}H shifts for each residue, although the peaks were present in the (H)CCH 3D spectrum. We did not attempt to assign the resonances of side-chain ^{15}N, and ^{1}H attached to side-chain ^{15}N or aromatic ^{13}C.

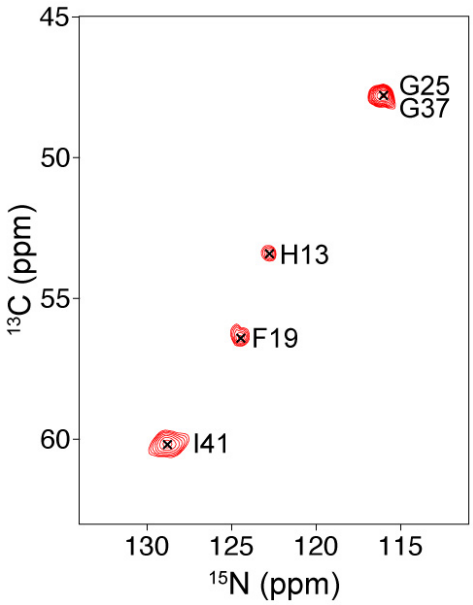

Figure S4. $^{13}C_{\alpha}/^{15}N$ 2D projection of ^{1}H-detected (H)CANH 3D spectrum with 3.6 ms HIGHLIGHT REDOR mixing of Val-reverse ^{13}C- and ^{15}N-labeled Aβ42 fibril as reported in a previous publication.[2] Experimental parameters used to record the spectrum can be found in the Materials and Methods section and Table S9.

Assignment validation by HIGHLIGHT REDOR for a Val-reverse ^{13}C- and ^{15}N-labeled Aβ42 fibril sample

We compared the assigned chemical shifts for uniformly ^{13}C- and ^{15}N-labeled Aβ42 fibril with the $^{13}C_{\alpha}$, ^{15}N and $^{1}H_{N}$ chemical shifts obtained in a 3D (H)CANH spectrum collected on a Val-reverse ^{13}C- and ^{15}N-labeled Aβ42 fibril sample with HIGHLIGHT REDOR mixing in a previous study (Figure S4 and Table S5).[2] According to the principle, 3D (H)CANH experiment using HIGHLIGHT REDOR mixing selectively detects the signal only for the residues located at the (i+1) position in the amino-acid sequence of Aβ42 compared to isotopically-unlabeled Val (i). Therefore, the signals observed in the 3D (H)CANH spectrum with HIGHLIGHT REDOR mixing should correspond to His-13, Phe-19, Gly-25, Gly-37 and Ile-41. However, by comparing the $^{13}C/^{13}C$ correlation 2D spectra of uniformly ^{13}C- and ^{15}N-labeled and Val-reverse ^{13}C- and ^{15}N-labeled Aβ42 fibrils, we realized that Val-reverse labeling

strategy unlabeled not only Val residues, but Leu residues as well (data are not shown). Hence, the signal observed at the ^{13}C shift of 53.4 ppm was the overlapped signals of His-13 and Met-35. Interestingly, the observed $^{13}C_{\alpha}$, ^{15}N and $^{1}H_{N}$ chemical shifts for Val-reverse ^{13}C- and ^{15}N-labeled Aβ42 fibril matched well with the corresponding shifts of uniformly ^{13}C- and ^{15}N-labeled Aβ42 fibril within ~1 ppm deviation for all the compared residues except for His-13/Met-35. For His-13/Met-35 signal, the maximum deviation of ~2 ppm was observed in the ^{15}N resonance.

ThT fluorescence spectroscopy for the brain-derived Aβ42 fibril sample

Aβ42 solution sample seeded with brain-derived material was prepared as described in the Materials and Methods section. Fluorescence measurements in the presence of ThT (Sigma-Aldrich) were performed on a Hitachi F-7000 fluorescence spectrometer with an excitation at 446 nm and an emission at 482 nm, as described previously.[3] A 10-μL aliquot of an Aβ42 fibril solution was diluted with 0.990 mL of 50 mM glycine buffer, pH 9.0 (Sigma-Aldrich), and the solution was then mixed with 10 μL of a 300 μM ThT solution. The final concentration of ThT was 3 μM. The lack of the lag time right after the incubation suggested the effectiveness of the seeding with the brain-derived Aβ fibril.

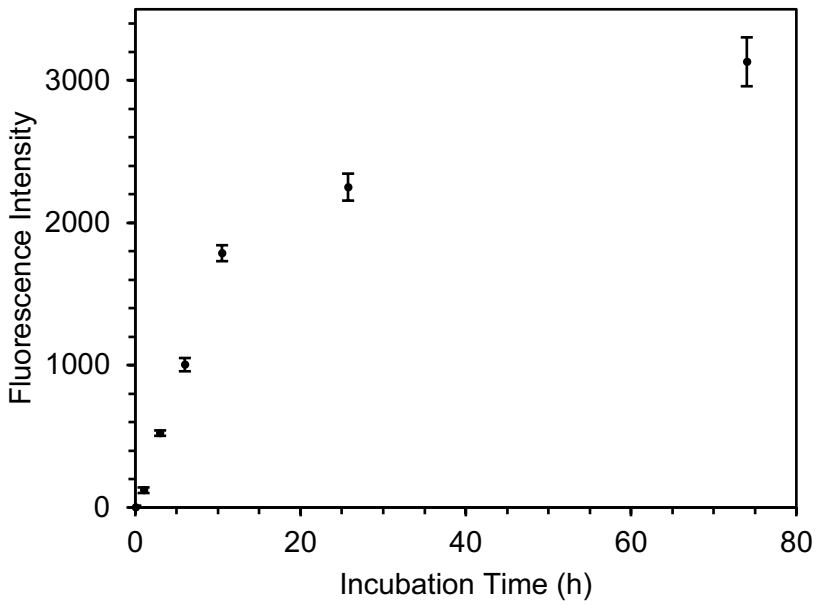

Figure S5. Incubation time dependence of ThT fluorescence of 40 μM Aβ42 solution seeded with 0.01% brain-derived Aβ fibril.

Supplementary Tables

Table S1. ^{13}C, ^{15}N and ^{1}H chemical shifts of brain-derived Aβ42

Residue	Chemical shift (ppm)										
	C_α	C_β	$C_{\gamma1}$	$C_{\gamma2}$	N	H_α	H_β	$H_{\gamma1}$	$H_{\gamma2}$	$H_{\delta1}$	H_N
F20`	56.5	42.8			133.7	5.09					8.91
F20``	56.7	42.3			120.0	4.85					8.82
F20```	57.0	40.2			114.6	5.19	2.94				7.80
A21`	49.5	20.7			132.3	5.19	0.89				8.39
A21``	49.4	22.7			119.7	5.14	0.95				8.25
A21```	52.8	20.3			126.7	4.03	1.27				9.36
A21````	49.7	22.9			134.2	5.72	0.95				8.61
V24`	58.3	36.1	22.7	21.1	121.5	5.56	1.55	0.59	0.59		7.31
V24``	59.3	35.5	20.2	20.2	121.1	4.89		0.48	0.48		8.19
V24```	59.8	34.3	21.5	19.8			1.75	0.47	0.47		
V24````	60.8	35.7	21.5	21.5	123.6	4.95	1.75	0.60	0.60		8.58
G25`	45.8				127.3	3.57					6.90
G25``	45.8				113.3	3.57					8.46
G25```	48.6				117.8	3.79					8.43
L34`	53.7	45.8			126.0	5.18	1.31			0.8	8.62
L34``	53.2	44.5			128.6	5.43				0.5	8.27
L34```	54.9	45.2				4.57				0.5	

Table S2. Difference between the ($\Delta\delta^{13}C_\alpha$ - $\Delta\delta^{13}C_\beta$) value of brain-derived Aβ42 fibril in this study and previously reported Aβ42 and Aβ40 fibrils

Residue	Difference of ($\Delta\delta^{13}C_\alpha$ - $\Delta\delta^{13}C_\beta$)[a] (ppm)								
	Brain-derived Aβ42[b, 4]		Aβ42[5]	Aβ42[6]	Aβ42[c]	Brain-derived Aβ40[7]	Aβ40[8]	E22Δ Aβ40[9]	D23N Aβ40[10]
F20`	-	-	-3.0	-0.1	-4.7	-9.1	0.6	-12.1	3.6
F20``	-	-	-2.3	0.6	-4.0	-8.4	1.3	-11.4	4.3
F20```	-	-	0.1	3.0	-1.6	-6.0	3.7	-9.0	6.7
A21`	-	-	-3.6	1.9	1.0	-9.7	1.4	3.0	2.1
A21``	-	-	-5.7	-0.2	-1.1	-11.8	-0.7	0.9	0.0
A21```	-	-	0.1	5.6	4.7	-6.0	5.1	6.7	5.8
A21````	-	-	-5.6	-0.1	-1.0	-11.7	-0.6	1.0	0.1
V24`	-	-	-1.3	0.8	-3.8	-2.9	-5.2	0.7	-5.2
V24``	-	-	0.3	2.4	-2.2	-1.3	-3.6	2.3	-3.6
V24```	-	-	2.0	4.1	-0.5	0.4	-1.9	4.0	-1.9
V24````	-	-	1.6	3.7	-0.9	0.0	-2.3	3.6	-2.3
G25`	0.9	0.5	-2.7	-3.2	-2.0	-1.0	-1.2	-3.1	-
G25``	0.9	0.5	-2.7	-3.2	-2.0	-1.0	-1.2	-3.1	-
G25```	3.7	3.3	0.1	-0.4	0.8	1.8	1.6	-0.3	-
L34`	-1.0	-0.2	-7.4	-1.2	0.6	-1.1	0.0	-0.4	0.0
L34``	-0.2	0.6	-6.6	-0.4	1.4	-0.3	0.8	0.4	0.8
L34```	0.8	1.6	-5.6	0.6	2.4	0.7	1.8	1.4	1.8

a. ($\Delta\delta^{13}C_\alpha$ - $\Delta\delta^{13}C_\beta$) value of brain-derived Aβ42 fibril in this study (ppm) – ($\Delta\delta^{13}C_\alpha$ - $\Delta\delta^{13}C_\beta$) value of previously reported Aβ42 and Aβ40 fibrils (or our recombinant Aβ42 fibril) (ppm). ($\Delta\delta^{13}C_\alpha$ – $\Delta\delta^{13}C_\beta$) denote the difference of the secondary ^{13}C chemical shifts of $^{13}C_\alpha$ and $^{13}C_\beta$, which are indicators of the secondary structures. Refs. 4–10 are found in the supplementary references at the end of SI.

b. Two sets of chemical shifts were reported for each isotope labeled residue. Chemical shifts of Phe-20, Ala-21 and Val-24 were not reported since they were not isotope labeled in the fibrils.

c. Uniformly ^{13}C- and ^{15}N-labeled recombinant Aβ42 fibril in this study.

Table S3. ^{13}C and ^{15}N chemical shifts of uniformly ^{13}C- and ^{15}N-labeled Aβ42 fibril

Residue	Chemical shift (ppm)[a]										
	^{13}CO	$^{13}C_\alpha$	$^{13}C_\beta$	$^{13}C_{\gamma1}$	$^{13}C_{\gamma2}$	$^{13}C_{\delta1}$	$^{13}C_{\delta2}$	$^{13}C_{\varepsilon1}$	$^{13}C_{\varepsilon2}$	$^{13}C_\zeta$	^{15}N
D1											
A2		52.9	20.2								
E3											
F4											
R5		54.9	30.2	28.3		44.8					
H6											
D7											
S8		57.1	67.0								
G9											
Y10		61.1	40.4			133.2	133.2	118.5	118.5	156.8	
E11	174.5	54.8	33.2	36.7							127.3
V12	175.3	60.4	35.0	21.6	20.6						122.0
H13	176.0	53.6	32.1	134.0			117.5				124.3
H14		55.5	32.7								122.3
Q15	175.4	56.5	30.5	35.4							118.4
K16	174.6	54.5	36.6	25.6		30.1					122.5
L17	174.5	55.1	44.7	30.1		26.3	25.1				128.6
V18	174.3	60.3	35.0	21.5	21.5						121.7
F19	173.3	56.4	42.3	137.6		131.3	131.3				124.4
F20	176.0	57.2	38.8	139.3							125.5
A21	176.2	50.7	22.9								126.7
E22[b]		54.6	33.0	36.4							122.4
D23	174.5	54.6	40.2	179.7							125.8
V24	176.2	59.9	33.9	21.7	20.9						122.3
G25	171.4	47.8									116.3
S26	173.6	55.8	65.4								117.1
N27	173.2	52.6	41.5	175.3							121.6
K28	174.5	55.8	34.7	26.0		30.0		42.2			127.0
G29	172.6	43.9									109.4
A30	175.7	49.8	21.8								128.5
I31	174.0	61.0	41.4	283	17.9	14.3					123.9
I32	177.4	57.7	40.7	28.3	18.6	13.9					127.2
G33[b]	171.6	48.6									119.8
L34	174.5	54.1	46.9	28.4		23.8	23.4				126.4
M35	173.6	53.5	38.1	31.7							124.8
V36	176.2	60.2	34.9	21.5	20.2						126.9
G37	172.2	48.2									116.2
G38	171.5	46.5									105.6
V39[b]	173.8	60.5	34.8	20.8	22.3						119.5
V40	172.7	60.4	35.0	21.0	21.5						127.5
I41	173.1	60.2	40.1	27.7	18.4	13.8					129.8
A42	181.4	51.9	21.6								134.9

Table S4. ^{1}H chemical shifts of uniformly ^{13}C- and ^{15}N-labeled Aβ42 fibril

Residue	Chemical shift (ppm)[a]							
	$^{1}H_{\alpha}$	$^{1}H_{\beta}$	$^{1}H_{\gamma1}$	$^{1}H_{\gamma2}$	$^{1}H_{\delta1}$	$^{1}H_{\delta2}$	$^{1}H_{\varepsilon1}$	$^{1}H_{N}$
D1								
A2	4.20	1.37						
E3								
F4								
R5	5.71	2.22	1.11					
H6								
D7								
S8	5.80	3.51						
G9								
Y10	4.98	2.84						
E11	5.47	1.93	2.52, 2.07					9.10
V12	5.38							8.32
H13	5.96	1.94						9.00
H14	5.46	2.23						8.71
Q15	5.64	2.65, 2.16	2.44					7.41
K16	5.61	2.07	1.44		1.68			8.44
L17	5.64	1.67, 1.41	2.06			0.95		8.96
V18	4.81							8.41
F19	5.02	3.04, 2.68						8.51
F20	5.44	3.05						9.34
A21	5.64	1.30						9.09
E22[b]	5.06	2.00	2.18					8.00
D23	5.52	2.60, 2.31						8.80
V24	5.02							8.82
G25	3.77, 4.34							9.23
S26	5.33	3.52						8.45
N27	5.64	3.23, 2.44						8.75
K28	4.30	2.12, 1.44	1.36		1.41		2.89	9.46
G29	3.80, 4.63							6.90
A30	5.50	0.94						8.76
I31	4.96	1.68	1.60	0.79	0.67			8.77
I32	5.48	1.61	1.38	0.66	0.57			9.27
G33[b]	3.93,3.93							8.69
L34	5.33	1.54, 1.36	1.54		0.81	0.64		8.23
M35	5.68	1.76	2.07					9.35
V36	5.18							8.59
G37	3.82, 4.27							8.96
G38	3.80, 3.80							7.81
V39[b]	5.13							8.05
V40	4.86							8.75
I41	4.84	1.70	1.50,1.40	0.57	0.69			9.02
A42	4.47	1.11						8.89

a. Errors of the assigned chemical shifts were approximately 0.2 ppm for ^{13}C and ^{15}N, and 0.07 ppm for ^{1}H.

b. A signal correspond to a minor species was observed for E22, G33 and V39 in ^{15}N-$^{1}H_N$ based 3D experiments.

Table S5. ^{13}C, ^{15}N and ^{1}H chemical shifts of Val-reverse ^{13}C- and ^{15}N-labeled Aβ42 fibril[2]

Residue	Chemical shift (ppm)		
	$^{13}C_\alpha$	^{15}N	$^{1}H_N$
H13	53.4 (53.6)	122.8 (124.3)	8.28 (9.00)
F19	56.4 (56.4)	124.5 (124.4)	8.44 (8.51)
G25	47.8 (47.8)	116.1 (116.3)	8.87 (9.23)
M35	53.4 (53.5)	122.8 (124.8)	8.28 (9.35)
G37	47.8 (48.2)	116.1 (116.2)	8.87 (8.96)
I41	60.2 (60.2)	128.8 (129.8)	8.74 (9.02)

Corresponding chemical shifts of the uniformly ^{13}C- and ^{15}N-labeled Aβ42 fibril are given in parenthesis.

Table S6. Torsion angles of uniformly ^{13}C- and ^{15}N-labeled Aβ42 fibril predicted by TALOS-N analysis[11]

Residue	ϕ	ψ
G9	104 ± 41*	174 ± 88*
Y10	-68 ± 9	137 ± 10
E11	-124 ± 15	145 ± 12
V12	-126 ± 8	137 ± 11
H13	-120 ± 10	135 ± 12
H14	-130 ± 14	143 ± 11
Q15	-111 ± 26	142 ± 13
K16	-133 ± 7	141 ± 11
L17	-116 ± 10	131 ± 7
V18	-122 ± 9	137 ± 9
F19	-118 ± 10	129 ± 8
F20	-102 ± 11	122 ± 8
A21	-123 ± 10	141 ± 13
E22	-131 ± 16	136 ± 13
D23	-83 ± 12	129 ± 9
V24	-127 ± 10	134 ± 17
G25	162 ± 71*	-161 ± 26*
S26	-137 ± 16	154 ± 5
N27	-117 ± 20	134 ± 9
K28	-115 ± 27*	140 ± 22*
G29	151 ± 40	-172 ± 19
A30	-127 ± 12	140 ± 10
I31	-116 ± 11	126 ± 9
I32	-118 ± 10	135 ± 14
G33	-158 ± 36*	-156 ± 32*
L34	-122 ± 12	132 ± 14
M35	-121 ± 7	132 ± 10
V36	-127 ± 6	125 ± 6
G37	59 ± 4	34 ± 6
G38	76 ± 7	11 ± 10
V39	-116 ± 9	137 ± 10
V40	-113 ± 12	127 ± 8
I41	-105 ± 7	129 ± 7

The angles marked with * were predicted with “Warn”.

Table S7. Acquisition parameters used for the NMR experiments of the synthetic and brain-derived Aβ42 fibrils

Sample	Synthetic Aβ42		Brain-derived Aβ42	
Experiment	(H)CH 2D	(H)CH 2D	(H)CCH 3D	(H)CANH 3D
Transfer 1	**^{1}H-^{13}C CP**	**^{1}H-^{13}C CP**	**^{1}H-^{13}C CP**	**^{1}H-^{13}C CP**
^{1}H RF field (kHz)	26.53	23.57	24.49	24.49
^{1}H shape	Rectangle	Rectangle	Rectangle	Rectangle
^{13}C RF field (kHz)	64.35	64.35	64.35	64.75
^{13}C shape	Tangent down (±20%)	Tangent down (±20%)	Tangent down (±20%)	Tangent down (±20%)
Time (ms)	0.50	0.50	0.80	0.60
Transfer 2	**^{13}C-^{1}H CP**	**^{13}C-^{1}H CP**	**RFDR**	**^{13}C-^{15}N CP**
^{1}H RF field (kHz)	29.19	23.57	-	-
^{1}H shape	Rectangle	Rectangle	-	-
^{13}C RF field (kHz)	63.56	64.35	83.33	68.00(±1.20)
^{13}C shape	Tangent up (±20%)	Tangent up (±20%)	-	Rectangle
^{15}N RF field (kHz)	-	-	-	24.00(∓1.20)
^{15}N shape	-	-	-	Rectangle
Time (ms)	0.40	0.40	2.00	2.04
Transfer 3	-	-	**^{13}C-^{1}H CP**	**^{15}N-^{1}H CP**
^{1}H RF field (kHz)	-	-	25.82	65.32
^{1}H shape	-	-	Rectangle	Tangent up (±20%)
^{13}C/^{15}N RF field (kHz)	-	-	63.56	23.11
^{13}C/^{15}N shape	-	-	Tangent up (±20%)	Rectangle
Time (ms)	-	-	0.40	0.50
t_1 increments	56	56	64	24
t_1 sweep width (kHz)	10.00	10.00	10.00	3.75
Max. t_1 acq. time (ms)	2.80	2.80	3.20	3.20
t_2 increments	512	512	64	30
t_2 sweep width (kHz)	100.00	100.00	10.00	2.31
Max. t_2 acq. time (ms)	2.56	2.56	3.20	6.50
t_3 increments	-	-	512	512
t_3 sweep width (kHz)	-	-	100.00	100.00
Max. t_3 acq. time (ms)	-	-	2.56	2.56
Total expt. time (h)	0.01	0.15	110.84	110.02
Number of scans	4	64	320	3072
Repetition delay (s)	0.08	0.08	0.20	0.13

Table S8. Acquisition parameters used for the NMR experiments of uniformly ^{13}C- and ^{15}N-labeled Aβ42 fibril in the main text

Experiment	(H)CCH 3D	(H)CA(CON)CAH 3D	(H)CANH 3D	(H)CA(CO)NH 3D
Transfer 1	**^{1}H-^{13}C CP**	**^{1}H-^{13}C CP**	**^{1}H-^{13}C CP**	**^{1}H-^{13}C CP**
^{1}H RF field (kHz)	22.36	21.55	20.41	20.41
^{1}H shape	Rectangle	Rectangle	Rectangle	Rectangle
^{13}C RF field (kHz)	66.67	68.53	66.67	66.67
^{13}C shape	Tangent down (±20%)	Tangent down (±20%)	Tangent down (±20%)	Tangent down (±20%)
Time (ms)	1.20	0.60	0.90	0.90
Transfer 2	**RFDR**	**DREAM**	**^{13}C-^{15}N CP**	**DREAM**
^{13}C RF field (kHz)	83.33	41.44	68.00(∓1.10)	42.58
^{13}C shape	-	Tangent up (±20%)	Rectangle	Tangent up (±20%)
^{15}N RF field (kHz)	-	-	27.00(±1.10)	-
^{15}N shape	-	-	Rectangle	-
Time (ms)	2.00	5.00	2.13	6.00
Transfer 3	**^{13}C-^{1}H CP**	**^{13}C-^{15}N CP**	**^{15}N-^{1}H CP**	**^{13}C-^{15}N CP**
^{1}H RF field (kHz)	22.36	-	62.54	-
^{1}H shape	Rectangle	-	Tangent up (±20%)	-
^{13}C RF field (kHz)	65.90	67.00(±1.00)	-	68.00(±0.90)
^{13}C shape	Tangent up (±20%)	Rectangle	-	Rectangle
^{15}N RF field (kHz)	-	18.50(∓1.00)	23.99	17.00(∓0.90)
^{15}N shape	-	Rectangle	Rectangle	Rectangle
Time (ms)	0.60	1.96	0.60	2.04
Transfer 4	-	**^{15}N-^{13}C CP**	-	**^{15}N-^{1}H CP**
^{1}H RF field (kHz)	-	-	-	62.54
^{1}H shape	-	-	-	Tangent up (±20%)
^{13}C RF field (kHz)	-	66.60(±1.20)	-	-
^{13}C shape	-	Rectangle	-	-
^{15}N RF field (kHz)	-	24.00(∓1.20)	-	23.99
^{15}N shape	-	Rectangle	-	Rectangle
Time (ms)	-	2.04	-	0.60
Transfer 5	-	**^{13}C-^{1}H CP**	-	-
^{1}H RF field (kHz)	-	20.70	-	-
^{1}H shape	-	Rectangle	-	-
^{13}C RF field (kHz)	-	67.79	-	-
^{13}C shape	-	Tangent up (±20%)	-	-
Time (ms)	-	0.30	-	-

t_1 increments	96	30	32	32
t_1 sweep width (kHz)	15.00	4.50	4.50	4.50
Max. t_1 acq. time (ms)	3.20	3.33	3.56	3.56
t_2 increments	96	30	42	42
t_2 sweep width (kHz)	15.00	4.50	2.65	2.65
Max. t_2 acq. time (ms)	3.20	3.33	7.93	7.93
t_3 increments	1024	768	1024	1024
t_3 sweep width (kHz)	100.00	100.00	100.00	100.00
Max. t_3 acq. time (ms)	5.12	3.84	5.12	5.12
Total expt. time (h)	14.62	37.78	31.53	68.12
Number of scans	16	320	512	720
Repetition delay (s)	0.25	0.32	0.10	0.15

Table S9. Acquisition parameters used for the NMR experiments of uniformly ^{13}C -and ^{15}N-labeled and Val-reverse ^{13}C -and ^{15}N-labeled Aβ42 fibrils in the Supplementary Information

Sample	Uniformly ^{13}C- and ^{15}N-labeled Aβ42				Val-reverse ^{13}C- and ^{15}N-labeled Aβ42
Experiment	(H)NH 2D	(H)CACONH 4D	(H)CX(CA)NH 3D	(H)CC 2D	(H)CANH 3D
Transfer 1	**^{1}H-^{15}N CP**	**^{1}H-^{13}C CP**	**^{1}H-^{13}C CP**	**^{1}H-^{13}C CP**	**^{1}H-^{13}C CP**
^{1}H RF field (kHz)	73.26	21.17	24.49	20.41	23.73
^{1}H shape	Tangent up (±20%)	Rectangle	Rectangle	Rectangle	Tangent up (±20%)
^{13}C/^{15}N RF field (kHz)	15.2	68.53	66.67	66.67	59.76
^{13}C/^{15}N shape	Rectangle	Tangent down (±20%)	Tangent down (±20%)	Tangent down (±20%)	Rectangle
Time (ms)	0.70	0.60	0.80	0.80	1.50
Transfer 2	**^{15}N-^{1}H CP**	**DREAM**	**TOBSY**	**RFDR**	**^{13}C-^{15}N CP**
^{1}H RF field (kHz)	62.63	-	-	-	-
^{1}H shape	Tangent up (±20%)	-	-	-	-
^{13}C RF field (kHz)	-	41.44	33.78	75.76	60.59
^{13}C shape	-	Tangent up (±20%)	-	-	Rectangle
^{15}N RF field (kHz)	22.42	-	-	-	21.38
^{15}N shape	Rectangle	-	-	-	Tangent up (±20%)
Time (ms)	0.70	5.00	14.93	1.42	6.00
Transfer 3	-	**^{13}C-^{15}N CP**	**^{13}C-^{15}N CP**	-	**^{15}N-^{1}H CP**
^{1}H RF field (kHz)	-	-	-	-	44.38
^{1}H shape	-	-	-	-	Tangent up (±20%)
^{13}C RF field (kHz)	-	66.00(±0.80)	65.00(±1.00)	-	-
^{13}C shape	-	Rectangle	Rectangle	-	-
^{15}N RF field (kHz)	-	18.50(∓0.80)	24.00(∓1.00)	-	29.46
^{15}N shape	-	Rectangle	Rectangle	-	Rectangle
Time (ms)	-	1.96	2.22	-	0.70
Transfer 4	-	**^{15}N-^{1}H CP**	**^{15}N-^{1}H CP**	-	-
^{1}H RF field (kHz)	-	63.03	63.67	-	-
^{1}H shape	-	Tangent up (±20%)	Tangent up (±20%)	-	-
^{15}N RF field (kHz)	-	23.57	20.75	-	-
^{15}N shape	-	Rectangle	Rectangle	-	-
Time (ms)	-	0.70	0.80	-	-
t_1 increments	52	22	72	320	32
t_1 sweep width (kHz)	2.73	4.50	12.86	45.00	5.00

Max. t_1 acq. time (ms)	9.53	2.44	2.80	3.56	3.20
t_2 increments	1024	8	32	2048	28
t_2 sweep width (kHz)	100.00	1.64	2.81	100.00	2.22
Max. t_2 acq. time (ms)	5.12	2.44	5.69	10.24	6.30
t_3 increments	-	22	1024	-	512
t_3 sweep width (kHz)	-	2.65	100.00	-	100.00
Max. t_3 acq. time (ms)	-	4.16	5.12	-	2.56
t_4 increments	-	1024	-	-	-
t_4 sweep width (ppm)	-	100.00	-	-	-
Max. t_4 acq. time (ms)	-	5.12	-	-	-
Total expt. time (h)	0.05	46.82	66.10	39.25	17.80
Number of scans	32	128	296	1024	108
Repetition delay (s)	0.07	0.23	0.26	0.40	0.60

Supplementary References

1. Zhou, D. H.; Rienstra, C. M., High-performance solvent suppression for proton detected solid-state NMR. *Journal of magnetic resonance (San Diego, Calif. : 1997)* **2008,** *192* (1), 167-172.

2. Wang, S.; Parthasarathy, S.; Xiao, Y.; Nishiyama, Y.; Long, F.; Matsuda, I.; Endo, Y.; Nemoto, T.; Yamauchi, K.; Asakura, T.; Takeda, M.; Terauchi, T.; Kainosho, M.; Ishii, Y., Nano-mole scale sequential signal assignment by 1H-detected protein solid-state NMR. *Chemical Communications* **2015,** *51* (81), 15055-15058.

3. Xiao, Y.; McElheny, D.; Hoshi, M.; Ishii, Y., Solid-State NMR Studies of Amyloid Materials: A Protocol to Define an Atomic Model of Aβ(1–42) in Amyloid Fibrils. In *Peptide Self-Assembly: Methods and Protocols*, Nilsson, B. L.; Doran, T. M., Eds. Springer New York: New York, NY, 2018; pp 407-428.

4. Qiang, W.; Yau, W.-M.; Lu, J.-X.; Collinge, J.; Tycko, R., Structural variation in amyloid-β fibrils from Alzheimer's disease clinical subtypes. *Nature* **2017,** *541* (7636), 217-221.

5. Xiao, Y.; Ma, B.; McElheny, D.; Parthasarathy, S.; Long, F.; Hoshi, M.; Nussinov, R.; Ishii, Y., Aβ(1–42) fibril structure illuminates self-recognition and replication of amyloid in Alzheimer's disease. *Nature Structural & Molecular Biology* **2015,** *22* (6), 499-505.

6. Gremer, L.; Schölzel, D.; Schenk, C.; Reinartz, E.; Labahn, J.; Ravelli, R. B. G.; Tusche, M.; Lopez-Iglesias, C.; Hoyer, W.; Heise, H.; Willbold, D.; Schröder, G. F., Fibril structure of amyloid-β(1–42) by cryo–electron microscopy. *Science* **2017,** *358* (6359), 116.

7. Lu, J.-X.; Qiang, W.; Yau, W.-M.; Schwieters, Charles D.; Meredith, Stephen C.; Tycko, R., Molecular Structure of β-Amyloid Fibrils in Alzheimer's Disease Brain Tissue. *Cell* **2013,** *154* (6), 1257-1268.

8. Petkova, A. T.; Yau, W.-M.; Tycko, R., Experimental Constraints on Quaternary Structure in Alzheimer's β-Amyloid Fibrils. *Biochemistry* **2006,** *45* (2), 498-512.

9. Schütz, A. K.; Vagt, T.; Huber, M.; Ovchinnikova, O. Y.; Cadalbert, R.; Wall, J.; Güntert, P.; Böckmann, A.; Glockshuber, R.; Meier, B. H., Atomic-Resolution Three-Dimensional Structure of Amyloid β Fibrils Bearing the Osaka Mutation. *Angewandte Chemie International Edition* **2015,** *54* (1), 331-335.

10. Sgourakis, Nikolaos G.; Yau, W.-M.; Qiang, W., Modeling an In-Register, Parallel "Iowa" Aβ Fibril Structure Using Solid-State NMR Data from Labeled Samples with Rosetta. *Structure* **2015,** *23* (1), 216-227.

11. Shen, Y.; Bax, A., Protein backbone and sidechain torsion angles predicted from NMR chemical shifts using artificial neural networks. *Journal of Biomolecular NMR* **2013,** *56* (3), 227-241.